Journal of Catalysis **188,** 252–260 (1999)
Article ID jcat.1999.2508, available online at http://www.idealibrary.com on IDEAL®

Acidity and *m*-Xylene Isomerization Activity of Large Pore, Zirconium-Containing Alumino-silicate with BEA Structure

Bhavana Rakshe, Veda Ramaswamy, and A. V. Ramaswamy*

Catalysis Division, National Chemical Laboratory, Pune 411 008, India

Received February 16, 1999; accepted March 29, 1999

A large pore, zirconium-containing alumino-silicate with BEA structure, Zr–Al-β ($SiO_2/ZrO_2 = 100$ and 50; $SiO_2/Al_2O_3 = 25$), has been synthesized hydrothermally using TEAOH as template and characterized by XRD, FTIR, and diffuse reflectance UV–visible spectral techniques to show that Zr^{4+} ions are isolated and are probably linked to the framework of the aluminosilicate of BEA structure. The FTIR studies of adsorbed pyridine, evacuated at different temperatures show an increase in Lewis as well as Brønsted acidity of Zr–Al-β samples in comparison to Zr-free Al-β and Zr-impregnated Al-β, having similar Al contents. The enhancement is probably the result of incorporation of Zr^{4+} ions into the β structure as $Si-O^{\delta-} \ldots Zr^{\delta+}$ linkages. The catalytic activity of Zr–Al-β samples is demonstrated in the isomerization of *m*-xylene at atmospheric pressure in a fixed bed reactor. The additional acidity of Zr–Al-β catalyst has been correlated with a marginal increase in the isomerization activity as well as selectivity to the isomerization products rather than the disproportionation products, particularly at temperatures below 500 K. © 1999 Academic Press

Key Words: **Zr–Al-beta zeolite; Zr-containing zeolite; acidity of Zr–Al-β; isomerization activity; isomerization of *m*-xylene; Zr-modified β zeolite.**

INTRODUCTION

We have recently reported the synthesis of medium-pore zirconium silicate molecular sieves with MFI and MEL structures. It was presumed that about 0.6–1.0 Zr atom per unit cell is located in the MFI and MEL framework, which showed good activity in the hydroxylation of phenol using aqueous H_2O_2 and selectivity for the formation of catechol and hydroquinone (1, 2). These mildly acidic catalysts also showed a remarkable activity in the vapor phase decomposition of 2-propanol and selectivity to propene and acetone at >473 K (3). However, their mild acid sites and relatively small pore openings of the structures limit the applications of such materials. It should be possible to overcome these limitations and improve the performance of Zr-containing molecular sieves by the synthesis of large pore structures such as zeolite beta (β). The possibility of synthesizing similar structures with other heteroatoms has attracted considerable attention recently. For example, Ti-, V-, and Sn-modified β zeolites have been shown to be useful as catalysts in the selective oxidation of a number of organic substrates (4–7). The methods of synthesis of Ti- and Sn-containing β zeolites were modified using dealuminated zeolite-β by many researchers (7, 8) to prepare Al-free Ti-β and Sn-β zeolites. These catalysts showed an enhanced activity and selectivity in the oxidation reactions with respect to the Al–Ti- and Al–Sn-β samples, respectively.

Zeolite β is of considerable interest due to its large micropore structure as well as high surface acidity and has found application in several reactions such as cracking, isomerization, alkylation, and disproportionation (9–12). Our aim is to incorporate Zr^{4+} ions in the framework of zeolite β and to investigate the effect of zirconium in the aluminosilicates on the acid properties and hence on the catalytic activity.

In the present report, we describe the synthesis of Zr-containing large pore aluminosilicates with BEA structure for the first time and compare its properties and catalytic activity with those of Zr-free Al-β and Zr-impregnated Al-β samples of similar Al content. The structural variations in these samples are characterized using different spectral techniques such as X-ray diffraction and diffuse reflectance (DR) UV–visible and FTIR spectroscopy. The intrinsic activity of zirconium is investigated in the isomerization of *m*-xylene at different contact times in the temperature range of 453–523 K. Additional Lewis as well as Brønsted acidities of Zr–Al-β samples, as demonstrated by pyridine adsorption studies, are correlated with a marginal increase in the activity and selectivity to isomerization products (*p*- and *o*-xylenes), particularly at temperatures below 500 K.

EXPERIMENTAL

Catalyst Preparation and Characterization

The Zr–Al-β zeolite samples were synthesized under hydrothermal conditions using gels with the following molar composition: SiO_2, x Na_2O, y ZrO_2, z Al_2O_3, 0.55 NEt_4OH, 30 H_2O, where $x = 0.02$–0.04, $y = 0.01$–0.02, $z = 0.04$, and NEt_4OH is tetraethylammonium hydroxide. In a typical preparation, 23.14 g of NEt_4OH (35% aqueous solution,

0021-9517/99 $30.00

Aldrich) was added slowly to 6 g of fumed silica (Sigma, S-5005, 99.8%) in 27 g of deionized water. After stirring for 1 h, 0.48 g of $ZrCl_4$ (Merck, 98%) in 5 g of water was added dropwise to the mixture under stirring. Then, 2.52 g of $Al_2(SO_4)_3 \cdot 16\,H_2O$ (Loba Chemie) dissolved in 5 g of water was added. Finally, 0.4 g of NaOH (Loba Chemie, 99%) in the remaining volume of water was added. After stirring for 1 h, the milky gel was transferred into a stainless steel autoclave and heated at 413 K for 10 days under static conditions. After completion of crystallization, the solid product was filtered, washed with deionized water, dried at 373 K, and calcined in air at 873 K for 10 h. Two such Zr–Al-β samples (A and B, respectively) were prepared with different Zr contents and similar Al contents ($SiO_2/ZrO_2 = 100$ and 50; $SiO_2/Al_2O_3 = 25$).

The Na form of the synthesized samples was ion exchanged three times with 1 M NH_4NO_3 solution at 363 K and recalcined at 873 K for 10 h to obtain the H form of Zr–Al-β samples. For comparison, Zr-free Al-β ($SiO_2/Al_2O_3 = 25$) and a Zr-impregnated Al-β ($SiO_2/ZrO_2 = 50$ and $SiO_2/Al_2O_3 = 25$) were also prepared. The latter was made by impregnating an Al-β sample with an aqueous solution of $ZrCl_4$ and then calcining at 823 K for 8 h. The synthesis of Zr–Al-β in the absence of sodium and with lower concentration of aluminium ($SiO_2/Al_2O_3 > 50$) was attempted, but the gel did not crystallize even after 30 days.

The calcined samples were characterized by XRD (Rigaku Model D-MAX III VC, Ni filtered Cu$K\alpha$ radiation), SEM (Leica Stereoscan Model 440), diffuse reflectance UV–visible spectroscopy (Shimadzu, UV–VIS spectrophotometer Model 2101 PC), and FTIR spectroscopy (Nicolet, Model 60 SXB). The elemental analysis was performed using ICP spectrometer (Jobin Yuon, Model JY-38 VHR) and XRF (Rigaku, Model 3070) methods. The micropore areas and micropore volumes were determined from the N_2 adsorption isotherms at liquid nitrogen temperature (Coulter Model 100CX Omnisorp). The monolayer volumes were taken at $p/p_o = 0.05$, where all micropores are filled up.

FTIR spectra of Zr–Al-β(B), Zr impregnated Al-β and Al-β samples were recorded between 4000 and 1300 cm^{-1} (hydroxyl and pyridine) regions. The samples were pressed into self-supported wafers with a radius (R) of 0.5 cm and a weight (W) of 7 mg and placed in the IR cell. The wafers were pretreated at 673 K for 3 h, *in vacuo* (1.33×10^{-4} Pa), and then equilibrated with pyridine (1.33×10^{3} Pa) after cooling to 373 K. All spectra (500 scans) were run at a resolution of 4 cm^{-1}, after subsequent desorption of the wafers for 1 h at different temperatures of 373, 473, 573, and 673 K.

Catalytic Studies

The isomerization of *m*-xylene was performed over Zr–Al-β molecular sieves with different Si/Zr atomic ratios in the temperature range of 453 to 523 K. These reactions were carried out in a fixed-bed downflow glass reactor (internal diameter = 13 mm) at atmospheric pressure. Prior to a typical catalytic run, the H form of the zeolite catalyst in the form of pellets (8×10 mesh size) was heated to 723 K in air for 2 h. The reactor was then cooled down to the reaction temperature under a flow of nitrogen. The contact times of the samples, expressed as W/F, with W as the weight of the catalyst and F the molar flow of *m*-xylene feed (Aldrich, 99.8%) at the reactor inlet, were kept between 1.06 and 4.25 h. The steady state conversions were calculated after 90 min. The analyses of the products were performed in a gas chromatograph (Shimadzu GC-14B) equipped with a flame ionization detector and a 2-m-long stainless steel column packed with 5% bentone and 5% diisodecylphthalate. The mass balances (99.5 wt%) were done on the basis of the weight of the products, i.e., the fractions collected after the reaction with respect to *m*-xylene fed. The feed used was 99.9% pure. The calibration was done with external standards of different concentrations prior to all GC analyses and corresponding response factors were used for processing the GC results.

For silynation, the catalyst (0.9 g) was exposed to a vaporized feed consisting of 45 wt% toluene, 48.5 wt% methanol and 6.5 wt% tetraethylorthosilicate at 473 K in a fixed bed downflow reactor. The coke formed during the deposition was burned off by heating the catalyst at 823 K in a flow of dry air. The *m*-xylene isomerization was subsequently carried out over the silynated catalyst.

RESULTS AND DISCUSSION

Characterization

The powder X-ray diffraction profiles of calcined samples are similar to Al-β (Fig. 1). The crystallinity was evaluated by a comparison of the area of the most intense diffraction peak in the 2θ range of 20°–24° to that of parent zeolite (Al-β) sample taken as 100% crystalline, after background subtraction (Table 1). It was observed that FWHM (full width of half-maximum intensity) for the first broad peak ($2\theta = 7.7°$) increases with an increase in the concentration of zirconium in BEA framework. This is a consequence of the decrease in the crystallite size, which is in agreement with an increase in the micropore surface area of Zr–Al-β samples.

The combination of sharp and broad features of the X-ray pattern of BEA structure due to the stacking disorder of the atomic planes complicates the interpretation of diffraction data by conventional methods. This interplanar fault probability (the probability of a change in the handedness of the stacking sequence), $\alpha = (I_b/I_n) = 0.1$–0.58 approximates polymorph A type structure (tetragonal crystal system), where I_b represents intensity of the first

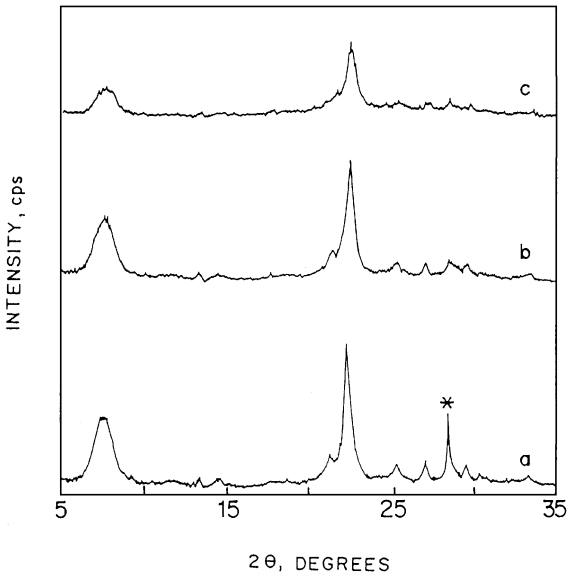

FIG. 1. X-ray diffraction profiles of calcined Al-β, Zr–Al-β (A), and Zr–Al-β (B) samples (curves a to c), respectively (*, Si peak).

broad peak at $2\theta = 7.7^\circ$ and I_n the intensity of the sharp peak at $2\theta = 22.5^\circ$ (13). All samples including Zr-free Al-β also showed $I_b/I_n = \approx 0.50$–0.57 which are found to be in favor of *polymorph A* structure. Therefore, unit cell parameters of the samples were determined by least squares fitting to the corrected *d* values with respect to silicon as an internal standard, based on a tetragonal system. There is a linear reduction along the *a* axis and an increase along the *c* axis. This results in a marginal change in unit cell volume with an increase of Zr content in the samples. These anisotropic changes in the unit cell parameters may be an indication of the different orientation of crystallites along a particular crystallographic axis, due to Zr-defects. As shown in Table 1, all XRD parameters of Zr-impregnated Al-β sample were found to be similar to those of Al-β sample. This shows clearly that extraframework Zr could not modify the properties of β zeolite in comparison to Zr–Al-β samples.

Scanning electron micrographs (not shown) confirmed the absence of any amorphous material around the crystals. The samples showed uniformly dispersed cuboid crystals with particle sizes of 0.5–1.0 μm. Furthermore, IR spectra in the region of framework vibrations were recorded to ascertain the high degree of crystallinity of Al-β, Zr–Al-β (A), Zr-impregnated Al-β, and Zr–Al-β (B) samples (Fig. 2, curves a to d, respectively), using the KBr pellet technique. All the spectra showed sharp features at 1232, 1098, 850, 580, 565, and 468 cm^{-1}, which are typical of zeolite beta structure (15). The band at 1232 cm^{-1}, due to asymmetric stretching vibrations of Si–O–*T* (*T* = Al, Zr) in Zr-free Al-β and Zr-impregnated Al-β (curves a and c) is shifted to lower wavenumbers of 1222 cm^{-1} in Zr–Al-β (B) sample (curve d) with increasing Zr content in the BEA framework. A characteristic band (shoulder) at $\sim$963 cm^{-1} is also observed in the Zr–Al-β as well as Al-β samples, which may be due to internal $Si\text{-}O^-$ defect sites (16).

The N_2 adsorption isotherms are characteristic of microporous materials. The micropore volumes are in the range of 0.18–0.20 mL g^{-1}. The micropore surface areas are in the range of 530 $m^2\,g^{-1}$ in comparison to a value of 452 $m^2\,g^{-1}$ obtained for Al-β sample. A small contribution of mesopore area is observed in the sample of Zr–Al-β (B) which has a higher Zr content (6.2%).

The diffuse reflectance UV spectra of Al-β, Zr-impregnated Al-β, Zr–Al-β (A), Zr–Al-β (B), and ZrO_2 samples (curves a to e, respectively) are shown in Fig. 3. An absorption at about 206 nm is attributed to the ligand-to-metal charge transfer involving isolated Zr(IV) atoms in tetrahedral coordination (curves c and d) (17, 18). There is a remarkable increase in the intensity of 206 nm band with Zr content in the BEA structure (16). These electronic transitions are clearly distinguishable from those in Zr-impregnated Al-β (curve b) and ZrO_2 (monoclinic symmetry) (curve e) which show absorptions at about 210 and 240 nm, respectively. A similar observation is reported by Blasco *et al.* for Ti-containing Al-β zeolite samples (19).

TABLE 1

Physico-chemical Characteristics of Zr–Al-β Samples

Sample	SiO_2/Al_2O_3 Gel	SiO_2/Al_2O_3 Product	SiO_2/ZrO_2 Gel	SiO_2/ZrO_2 Product	XRD parameters: Crystallinity (%)	FWHM	Crystallite size[a] (Å)	$\alpha^b = I_b/I_n$	a (Å)	b (Å)	UCV (Å^3)	Micropore area ($m^2\,g^{-1}$)	Mesopore area[c] ($m^2\,g^{-1}$)
Al-β	25	26	—	—	100	1.41	57.1	0.55	12.4938	26.3405	4112	352	13.0
Zr–Al-β (A)	25	27	100	115	88	1.48	54.1	0.57	12.4670	26.4404	4110	501	28.8
Zr–Al-β (B)	25	27	50	63	75	1.59	50.5	0.47	12.4241	26.4519	4083	530	33.0
Zr-impreg. Al-β	25	26	—	52	97	1.42	56.4	0.58	12.4935	26.3400	4111	490	3.2

[a] Calculated using Debye–Scherrer equation, D (Å) $= k\lambda/\sqrt{b}\cos\theta$ (14).
[b] I_b, intensity of broad peak at $2\theta = 7.7^\circ$; I_n, intensity of sharp peak at $2\theta = 22.5^\circ$.
[c] From the *t* plot.

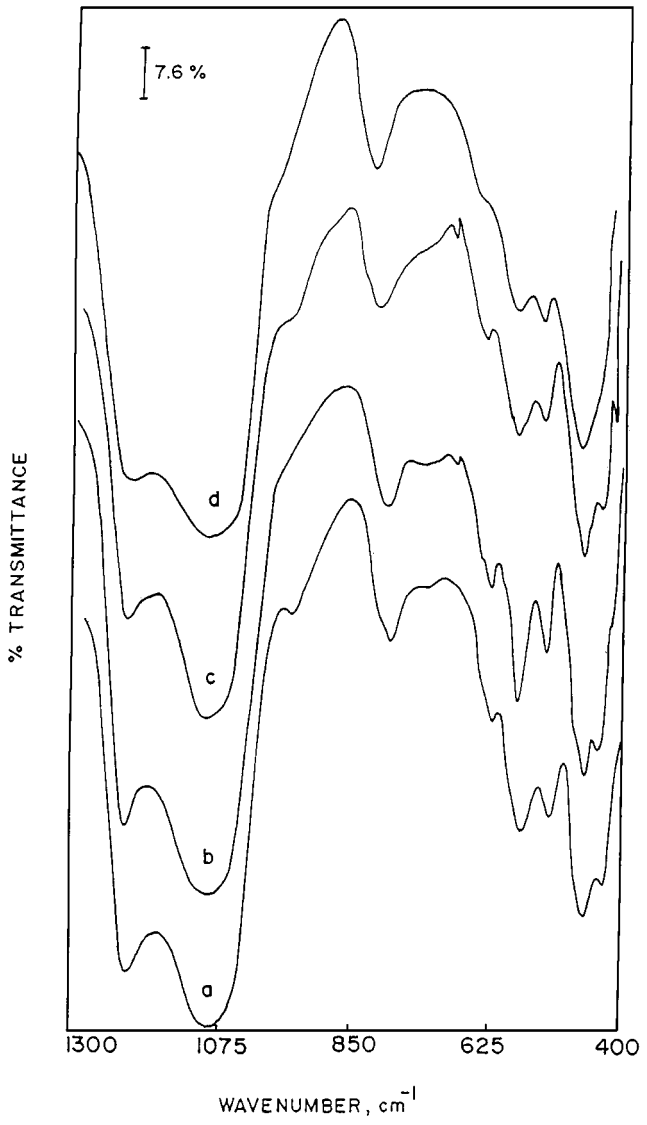

FIG. 2. Infrared spectra of Al-β, Zr–Al-β (A) and Zr-impregnated Al-β and Zr–Al-β (B) samples (curves a to d, respectively).

However, no band at 240 nm corresponding to zirconia was detected in our samples (curves c and d).

Infrared spectra of Al-β, Zr-impregnated Al-β, and Zr–Al-β (B) samples in the hydroxyl region are shown in Fig. 4 (curves a to c, respectively). The spectrum of Zr–Al-β (curve c) showed relatively higher integrated intensities than the spectra of Al-β (curve a) and Zr-impregnated Al-β (curve b) samples in the region of 4000–3000 cm^{-1}. All spectra exhibited the classical absorptions at 3607 ($Si–OH^+$–Al) and 3731 cm^{-1}, which are due to framework bridging acidic OH and terminal silanols, respectively. A weak band at 3780–3775 cm^{-1} is attributed to extraframework hydroxyl groups. The band at 3660 cm^{-1} due to alumina-like species is not observed. The broad band at 3700–3000 cm^{-1} is generally assigned to H-bonded SiOH groups which may

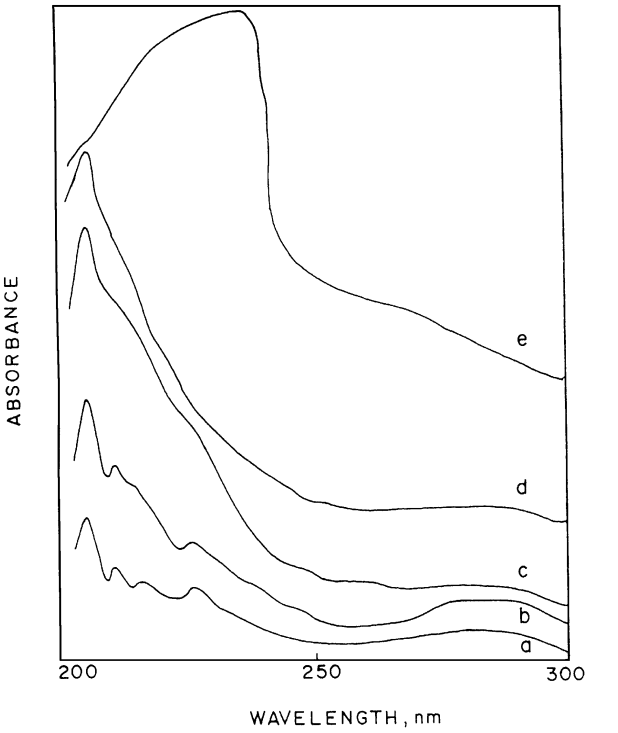

FIG. 3. Diffuse reflectance UV spectra of Al-β, Zr-impregnated Al-β, Zr–Al-β (A), Zr–Al-β (B), and ZrO_2 samples (curves a to e, respectively).

be located in the hydroxyl nests or framework defect sites (20).

The nature of acidic sites in the samples of Zr–Al-β (B), Zr-impregnated Al-β, and Al-β samples (Figs. 5A to 5C, respectively) was characterized by adsorption of pyridine

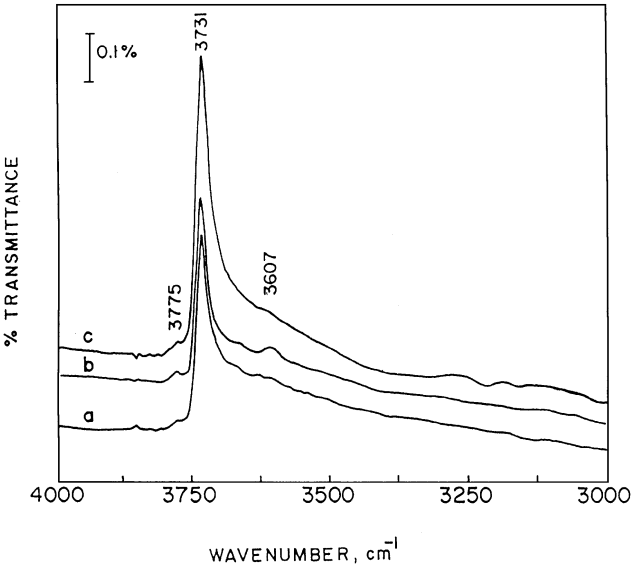

FIG. 4. Infrared spectra of Al-β, Zr-impregnated Al-β, and Zr–Al-β (B) samples in the hydroxyl region, after evacuation at 673 K (curves a to c, respectively).

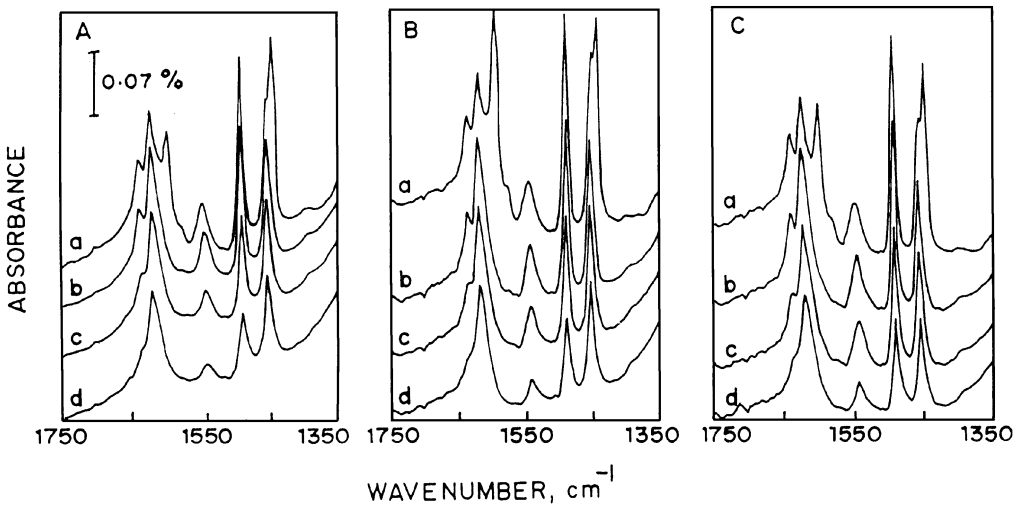

FIG. 5. (A) Infrared spectra of pyridine adsorbed on the Zr–Al-β, (B) Zr-impregnated Al-β, and (C) Al-β samples after evacuation at the different temperatures of 373, 473, 573, and 673 K (curves a to d, respectively).

(py) at 373 K (curve a) and stepwise desorption at increasing temperatures of 473, 573, and 673 K (curves b to d, respectively). In the range of 1750–1300 cm^{-1} of the spectra of all samples, chemisorbed py was revealed by the usual set of bands: the band at 1540 cm^{-1}, indicative of pyridinium ion (pyH^+), and the bands at 1445 and 1618 cm^{-1}, related to Lewis-bonded py. The superposition of signals of both protonic acid sites (N^+–H) as well as on Lewis acid adsorbed species at 1490 cm^{-1} is also observed (21). The coordinately bonded pyridine (1445 cm^{-1}) and some pyridinium ions (1540 cm^{-1}) are retained even after evacuation of the samples at 673 K. Also, the higher intensities of the bands at 1620 and 1445 cm^{-1} indicate that the surface acidity of the samples is predominately of the Lewis type.

For the determination of the fractions of Brønsted and Lewis acid sites on the surface, the integrated intensities of PyH^+ and PyL bands (1540 and 1445 cm^{-1}, respectively) were estimated, after background subtraction. A plot of these values at different desorption temperatures is shown in Fig. 6. The integrated intensities of Brønsted and Lewis acid sites of these samples after evacuation at different desorption temperatures show that Zr–Al-β sample appears significantly more acidic than either Zr-free Al-β or the Zr-impregnated Al-β samples.

The concentrations of Brønsted and Lewis acid sites were calculated from the integrated intensities of PyH^+ and PyL bands and the molar extinction coefficients of these bands (1.67 and 2.22 cm μmol^{-1}, respectively) (22). A comparison of these values with the concentration of total acid sites (in forms of Al and Zr atoms in millimoles per gram of the sample) is presented in Table 2. It indicates that incorporation of Zr^{4+} ions in Al-β structure generates additional acidity due to the strong polarization of possible $Si–O^{\delta-} \ldots Zr^{\delta+}$ linkages. Thus, it verifies that there are two types of linkages viz., Si–O . . . Zr and Si–O . . . Al, which due to their different polar nature play an important role in the acid site distribution of Zr–Al-β samples.

In our earlier reports, the IR spectra of py adsorbed on the samples of Zr-silicates with MEL structure have been interpreted as an indication that the tetrahedral Zr in the silicalite lattice bears a $\delta+$ charge so that the O . . . Zr bond may be viewed as a Lewis acid–base pair (1). We have recently offered a similar interpretation in the case of Zr-silicates with MFI structure by analyzing the electronic structure of suitable cluster models to study the interaction of lone pair of py with Zr 4*d* orbitals. It was found that the binding energy of py with surface hydroxyl groups is less compared to that of py when it is coordinated to Zr^{4+} ions due to the stabilization of an e_g orbital in the possible tetrahedral coordination (2).

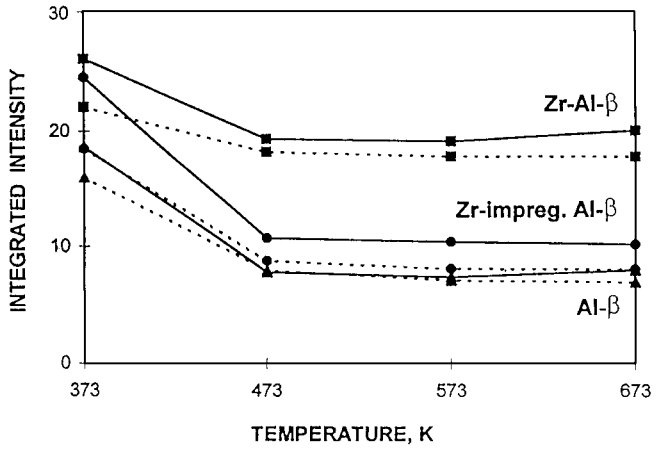

FIG. 6. A plot of integrated intensities of the bands 1540 cm^{-1} (Brønsted bound pyridine) and 1445 cm^{-1} (Lewis bound pyridine) as shown by dotted and solid lines, respectively, vs desorption temperatures of Al-β (▲) and Zr-impregnated Al-β (●) and Zr–Al-β (B) (■) samples.

TABLE 2

Effect of Different Desorption Temperatures on the Brønsted and Lewis Acidity

Sample	Desorption temperature (K)	I_{1540}/I_{1445}	Concentration (mmol g^{-1} of sample) B[a]	L[a]	B + L	(Al + Zr)[b]
Al-β	373	0.86	1.07	0.94	2.01	2.56
	473	1.02	0.53	0.39	0.92	(only Al)
	573	0.96	0.47	0.36	0.83	
	673	0.87	0.46	0.39	0.85	
Zr-impreg. Al-β	373	0.80	1.24	1.16	2.40	3.00
	473	0.82	0.58	0.53	1.11	
	573	0.78	0.53	0.51	1.04	
	673	0.79	0.54	0.50	1.04	
Zr–Al-β (B)	373	0.90	1.48	1.23	2.71	2.90
	473	0.94	1.21	0.96	2.17	
	573	0.93	1.18	0.95	2.13	
	673	0.89	1.18	0.99	2.17	

[a] Concentration of pyridine adsorbed on Brønsted (B) and Lewis (L) acid sites per gram of sample, respectively, using Beer's law: ($C = \varepsilon \times I A \times \pi R^2/W$).

[b] Concentration of Al and Zr atoms (calculated from molar output Si/Al and Si/Zr ratios) per gram of the sample.

Catalytic Studies

The isomerization of *m*-xylene to *p*- and *o*-isomers is an important petrochemical process (23). This reaction is widely used in the laboratory to characterize the zeolites with 10- and 12-membered rings, such as ZSM-5 and mordenite on the basis of their different shapes and dimensions of the intracrystalline cavities (24–26). The isomerization to disproportionation selectivity is determined by the strong isolated acid sites which are present in the cavities that allow the formation of at least one of the possible bimolecular transition state complexes for disproportionation, in the group of 12-membered ring zeolites (27). Here, we have estimated the values of selectivities toward isomerization (I) and disproportion (D) products with a comparison of the acidity of Zr–Al-β (B) and Al-β samples.

Table 3 summarizes the effect of different temperatures in the range of 453–523 K on the product distribution of Al-β, Zr-impregnated Al-β, and Zr–Al-β (B) catalysts, at a contact time of 1.06 h. The catalytic activity of Zr–Al-β (B) sample is marginally higher than that of Al-β and it increases further with temperature. It was observed that the formation of isomerization products, i.e., *p*- and *o*-xylenes, is favored at lower temperatures. At higher temperatures, however, the selectivity for the disproportionation products, i.e., toluene and trimethylbenzenes is enhanced with a loss in the selectivity for isomerization products. As the temperature increases (>523 K), the conversion of *m*-xylene increases rapidly and reaches equilibrium values.

The *p*-/*o*-xylene ratio in the products is about 1.0–1.4, suggesting that there is no diffusion controlled product shape selectivity, as the pores are large enough to allow rapid diffusion of the xylene isomers. In contrast to 10-membered ring zeolites, the *p*/*o*-selectivity in 12-membered ring zeolites is not influenced by diffusion but by the transition-state shape selectivity (28). Martens *et al.* have reported the values of *p*/*o*-selectivity to be of 1.0–1.4 for various 12-membered ring zeolites with mono-, bi-, and tridimensional pore systems with or without lobes and/or intersections (29). The value of *p*/*o*-selectivity in our sample

TABLE 3

Effect of Temperature on the Product Distribution in the Isomerization of *m*-Xylene[a]

Catalyst	Temperature (K)	*m*-Xylene conv. (mol%)	Product selectivity (mol%) *p*-xylene	*o*-xylene	I^b (total)	Toluene	Trimethylbenzenes 1,3,5-	1,2,4-	1,2,3-	D^c (total)	*I*/*D*
Al-β	453	5.0	41.5	40.5	82.0	10.1	1.8	6.0	0.1	18.0	4.6
	473	6.3	39.7	39.7	79.4	10.3	3.2	6.7	0.4	20.6	3.9
	498	15.0	43.3	38.0	81.3	8.9	3.3	6.0	0.5	18.7	4.3
	523	33.6	40.3	35.0	75.3	10.4	3.0	10.3	1.0	24.7	3.0
Zr–impreg. Al-β	453	1.0	56.0	23.2	79.2	20.8	0.0	0.0	0.0	20.8	3.8
	473	4.2	43.0	33.9	76.9	12.9	1.2	9.0	0.0	23.1	3.3
	498	8.2	38.4	35.4	73.8	13.2	2.6	10.1	0.4	26.2	2.8
	523	30.5	35.8	32.6	68.4	14.2	4.6	11.5	1.1	31.5	2.2
Zr–Al-β (sample B)	453	5.7	53.0	41.7	94.7	3.5	0.0	0.0	0.0	5.3	17.9
	473	8.5	51.7	43.6	95.3	4.7	0.0	0.0	0.0	4.7	20.3
	498	20.0	52.5	38.0	91.5	5.0	0.0	3.5	0.0	8.5	10.8
	523	34.1	41.9	34.3	76.2	12.3	3.2	8.2	0.1	23.8	3.2

[a] Contact time, 1.06 h.

[b] Selectivity for isomerization products.

[c] Selectivity for all disproportionation products.

TABLE 4

Effect of Different Contact Times on the Conversion and Selectivities of Isomerization and Disproportionation Products at Various Temperatures

		Contact time (h)											
		1.06			1.42			2.12			4.25		
Catalyst	Temparature (K)	*m*-Xylene conv. (mol%)	Selectivity I^a	D^b	*m*-Xylene conv. (mol%)	Selectivity *I*	*D*	*m*-Xylene conv. (mol%)	Selectivity *I*	*D*	*m*-Xylene conv. (mol%)	Selectivity *I*	*D*
Zr–Al-β (B)	453	5.7	94.7	5.3	7.4	82.4	17.6	11.1	68.5	31.5	13.8	65.2	34.8
	473	8.5	95.3	4.7	15.3	79.7	20.3	18.8	64.4	35.6	31.9	60.8	39.2
	498	20.0	91.5	8.5	30.2	76.8	23.2	36.0	66.4	33.6	47.0	57.4	42.6
	523	34.1	76.2	23.8	40.8	71.3	28.7	49.4	57.7	42.3	56.6	55.2	46.8
Al-β	453	5.0	82.0	18.0	6.5	77.0	23.0	9.0	61.1	38.9	10.1	65.8	34.2
	473	6.3	79.4	20.6	12.0	74.2	25.8	15.5	60.6	39.4	28.5	54.0	45.8
	498	15.0	81.3	18.7	25.3	59.3	40.7	30.5	65.6	34.4	43.0	55.8	44.2
	523	33.6	75.3	24.7	39.4	58.9	41.1	44.6	55.2	44.8	50.1	45.2	54.8

[a] *I* (Isomerization products) = $\sum$ mol% selectivities of *p*- and *o*-xylenes.
[b] *D* (Disproportionation products) = $\sum$ mol% selectivities of toluene and trimethylbenzenes.

of zeolite β was found in the range of 1.0–1.2, in agreement with the presence of 12-membered rings. However, in Zr–Al-β catalyst, the formation of *p*-xylene is favored (*p*/*o*-selectivity = 1.2–1.4). It could be due to steric hindrance exerted by the framework in the formation of *o*-isomers. One possibility is that the protonation of *m*-xylene at the least accessible C_2 atom, leading to *o*-xylene formation, is sterically hindered. Preferred protonation at C_4 and C_6 could explain the higher *p*-selectivity of Zr–Al-β catalyst. Another possibility is that the size and shape of the pores hinders the formation and rearrangements of some of the intermediate species. At this moment, it is not possible to distinguish between the different possibilities, especially because the positioning of the catalytic intermediates in the channels is unknown.

A similar trend was observed for the distribution of products in both the catalysts, except the formation of trimethylbenzenes over Zr–Al-β catalyst, which occurs only at >498 K, resulting in a significant decrease in the isomerization to disproportionation (I/D) ratios (17.9 and 3.2 at 5.7 and 34.1 mol% conversions, respectively). The 1,3,5- to 1,2,4-trimethylbenzenes ratio in the product is 0.3–0.4, which is similar to the values reported already, at a conversion level of about 10% at 623 K for beta catalyst (28, 29).

In order to eliminate or poison the nonselective acid sites, impregnation of Al-β with ZrO_2 at the external surface was attempted, referred to as Zr-impregnated Al-β. It allowed an overall decrease in the activity (15.0 to 8.2 mol% at 498 K) as well as isomerization selectivity (75.3 to 68.4 mol% at around 30.0 mol% conversion) of Al-β sample, as shown in Table 3. However, Zr–Al-β catalyst showed a higher activity (20.0 mol% at 498 K) and isomerization selectivity (76.2 mol% at around 30.0 mol% conversion). These results clearly demonstrate the higher intrinsic activity of (framework) Zr in Zr–Al-β in comparison to the extraframework Zr in Zr-impregnated Al-β sample.

The effect of different contact times (1.06–4.25 h) of the catalysts on the conversion and selectivities of isomerization and disproportionation at various temperatures was studied and the data are given in Table 4. The conversion of *m*-xylene over Zr–Al-β catalyst increases with an increase in contact time and temperature while the selectivity of isomerization products is maximum at the lower contact time and at 453 K. At lower temperature and lower contact time, the conversions of *m*-xylene are not so high and consequently, the differences in the isomerization and disproportionation selectivities are more significant. The conversion increases rapidly with increase in temperature and approaches equilibrium values.

The rate constants were determined from the plot of mol% conversions of *m*-xylene vs contact time at different temperatures in the range of 453–523 K. From the slope of Arrehenius plot (log *r* vs $1/T$ K^{-1}) using linear regression method, the apparent activation energy values (E_a) were evaluated as follows (30):

$$\text{Slope} = -E_a/2.303\ R,$$

where $R = 8.314$ joules deg^{-1} mol^{-1}. The apparent activation energy for isomerization of *m*-xylene over Zr–Al-β catalyst is marginally lower ($E_a = 36.8$ kJ/mole) than observed over the Zr-free Al-β sample ($E_a = 38.9$ kJ/mol).

Besides pore size distribution, several other explanations have been proposed to explain the differences in isomerization and disproportionation selectivity in 12-membered ring zeolites. One hypothesis is related to the presence of

appropriately positioned Lewis acid center with respect to Brønsted acid sites, which may strengthen the acidity of these Brønsted acid sites (31). It has been suggested that disproportionation requires stronger acid sites than isomerization. Siliceous zeolites contain stronger Brønsted acid sites than high-alumina containing zeolites and show a significant activity for disproportionation. The presence of an appropriately positioned Lewis acid center with respect to Brønsted acid sites may strengthen the acidity of these Brønsted acid sites. Similarly, Zr, which itself is a Lewis acid, seems to enhance the overall Lewis acidity of Al-β zeolite. Thus it may alter the acid site distribution of Al-β sample in such a way that results in a lower selectivity for disproportionation than for isomerization. The higher selectivity for isomerization in Zr-Al-β sample is correlated with the strong Lewis as well as Brønsted acid sites over and above those present in Al-β samples.

The disproportionation reaction is a bimolecular reaction, occurs via 1,1-diphenylmethane intermediates that are bulkier than the reagent and product molecules. The acid sites located at the channel opening or preferably at the external surface of the zeolite crystals may play an important role in the formation of these intermediates (32). In order to passivate these external acid sites, we attempted to modify the samples with a deposition of a silica layer by means of chemical vapor deposition (CVD) technique using tetraethylorthosilicate (TEOS) (33, 34). In the silynated samples, silica covers the external surface, leaving the intrinsic active sites within the channels unperturbed (35). The effect of silynation on the conversion and selectivities in the isomerization of *m*-xylene is illustrated in Table 5. Silynation of the samples, in general, decreases the conversion of *m*-xylene at all temperatures. However, the silynated Zr–Al-β (B) (SiO_2 loading = 1.5 wt%) sample showed a significant increase in the conversions of *m*-xylene (29.0 mol%) as compared to the silynated Al-β catalyst (10.5 mol% at 473 K) at similar SiO_2 loading. After silynation, there is an increase in the isomerization selectivity in both the samples, as observed in the case of H-ZSM-5 catalyst. The selectivity for isomerization of the silynated Zr–Al-β sample is more pronounced ($\sum I = 77.2$ mol%) than that observed before silynation of the samples ($\sum I = 60.8$ mol%) at around 30.0 mol% conversions. Thus, it is evident that the enhancement in the activity as well as the isomerization selectivity of Zr–Al-β catalyst in the reaction is due to Zr and Al metal atoms, which are present inside the micropore system.

TABLE 5

Effect of Silynation on the Conversion and Selectivities in the *m*-Xylene Isomerization Reaction[a]

Catalyst	Reaction temperature (K)	453	473	498
Al-β (before silynation)	*m*-Xylene conv. (mol%)	10.1	28.5	43.0
	$\sum I^b$	65.8	54.0	55.8
	$\sum D^c$	34.2	45.8	44.2
Al-β (after silynation)	*m*-Xylene conv. (mol%)	4.8	10.5	34.0
	$\sum I$	83.0	74.4	68.5
	$\sum D$	17.0	25.6	31.5
Zr–Al-β (B) (before silynation)	*m*-Xylene conv. (mol%)	13.8	31.9	47.0
	$\sum I$	65.2	60.8	57.4
	$\sum D$	34.8	39.2	42.6
Zr–Al-β (B) (after silynation)	*m*-Xylene conv. (mol%)	4.4	29.0	42.0
	$\sum I$	90	77.2	70.0
	$\sum D$	10	22.8	30.0

[a] Contact time, 4.25 h.

[b] mol% selectivities of *p*- and *o*-xylenes (isomerization).

[c] mol% selectivities of toluene and trimethylbenzenes (disproportionation).

CONCLUSION

Two samples of zirconium-containing aluminium beta samples have been prepared and characterized by different techniques. These are compared with Zr-free Al-β and Zr-impregnated Al-β samples for different properties. Significant is the enhancement of acidity of Zr–Al-β by incorporation of Zr^{4+} ions probably in the lattice. It is presumed that Zr^{4+} Lewis acid sites may strengthen the Brønsted acid sites (due to Al^{3+} ions) and hence influence the isomerization of *m*-xylene. A marginal increase in *m*-xylene conversion and selectivity advantages for the isomerization products are noted with Zr–Al-β samples. Silynation studies further confirm the enhancement of activity and isomerization selectivity of Zr–Al-β catalysts.

ACKNOWLEDGMENTS

Our thanks are due to Dr. S. G. Hegde for FTIR spectra of pyridine adsorbed on samples. B.R. is grateful to the CSIR, New Delhi, for a research fellowship.

REFERENCES

1. Rakshe, B., Ramaswamy, V., and Ramaswamy, A. V., *J. Catal.* **163**, 503 (1996).
2. Rakshe, B., Ramaswamy, V., Hegde, S. G., Vetrivel, R., and Ramaswamy, A. V., *Catal. Lett.* **45**, 4 (1997).
3. Rakshe, B., Ramaswamy, V., and Ramaswamy, A. V., Paper presented at the First Conference of the Indo-Pacific Catalysis Association (IPCAT 1), Cape Town, South Africa, January 26–28, 1998.
4. Corma, A., Camblor, M. A., Esteve, P., Martínez, A., and Pérez-Pariente, J., *J. Catal.* **145**, 151 (1994).
5. Camblor, M. A., Corma, A., Martínez, A., and Pérez-Pariente, J., *J. Chem. Soc. Chem. Commun.* 589 (1992).
6. Sen, T., Chatterjee, M., and Sivasanker, S., *J. Chem. Soc. Chem. Commun.* 207 (1995).
7. Mal, N. K., and Ramaswamy, A. V., *Chem. Commun.* 425 (1997).
8. Camblor, M. A., Costantini, M., Corma, A., Gilbert, L., Esteve, P., Martínez, A., and Valencia, S., *Chem. Commun.* 1339 (1996).
9. Bonetto, L., Camblor, M. A., Corma, A., and Pérez-Pariente, J., *Appl. Catal.* **82**, 37 (1992).

10. Lapierre, R. B., Partridge, R. D., Chen, N. Y., and Wong, S. S. F., US patent, 4 501 926, 1983.
11. Reddy, K. S. N., Rao, B. S., and Shiralkar, V. P., *Appl. Catal.* **95**, 53 (1993).
12. Tsai, T. C., Ay, C. L., and Wang, I., *Appl. Catal.* **77**, 199 (1991).
13. Newsam, J. M. J., Treacy, M. M., Koetsier, W. T., and De Gruyter, C. B., *Proc. R. Soc. London A* **420**, 375 (1988).
14. Bish, D. L., and Post, J. E., *in* "Reviews in Mineralogy," Vol. 20, p. 204. The Mineralogical Society of America, Washington, DC, 1989.
15. Pérez-Pariente, J., Martens, J. A., and Jacobs, P. A., *Appl. Catal.* **31**, 35 (1987).
16. Camblor, M. A., Corma, A., Mifsud, A., and Pérez-Pariente, J., *Stud. Surf. Sci. Catal.* **105**, 341 (1997).
17. Wang, G. R., Wang, X. Q., Wang, X. S., and Yu, S. X., *Stud. Surf. Sci. Catal.* **83**, 67 (1994).
18. Tuel, A., Gontier, S., and Teissier, R., *Chem. Commun.* 651 (1996).
19. Blasco, T., Camblor, M. A., Corma, A., and Pérez-Pariente, J., *J. Am. Chem. Soc.* **115**, 11806 (1993).
20. Jia, C., Massiani, P., and Barthomeuf, D., *J. Chem. Soc. Faraday Trans.* **89**, 3663 (1993).
21. Miller, T. M., and Grassian, V. H., *Catal. Lett.* **46**, 213 (1997).
22. Emeis, C. A., *J. Catal.* **141**, 347 (1993).
23. Dwyer, F. W., Lewis, P. J., and Schneider, F. M., *Chem. Eng.* **83**, 98 (1976).
24. Dewing, J., *J. Mol. Catal.* **27**, 25 (1984).
25. Weisz, P. B., *Pure Appl. Chem.* **52**, 2091 (1980).
26. Csicsery, S. M., *Zeolites* **4**, 202 (1984).
27. Pérez-Pariente, J., Sastre, E., Fornes, V., Martens, J. A., Jacobs, P. A., and Corma, A., *Appl. Catal.* **69**, 125 (1991).
28. Martens, J. A., Pérez-Pariente, J., Sastre, E., Corma, A., and Jacobs, P. A., *Appl. Catal.* **45**, 85 (1988).
29. Kumar, R., and Reddy, K. R., *Microporous Mater.* **3**, 195 (1994).
30. Maron, S. H., and Prutton, C. F., "Principles of Physical Chemistry," 4th ed., p. 572. 1969.
31. Poutsma, M. L., *in* "Zeolite Chemistry and Catalysis" (J. A. Rabo, Ed.), ACS Monograph 171, p. 437. American Chemical Society, Washington, DC, 1976.
32. Benazzi, E., De Tavernier, S., Beccat, P., Joly, J. F., Nedez, C., Choplin, A., and Basset, J. M., *Chemtech* **24**, 13 (1994).
33. Hibino, T., Niwa, M., and Murakami, Y., *J. Catal.* **128**, 551 (1991).
34. Weber, R. W., Fletcher, J. C. Q., Möller, K. P., and O'Conner, C. T., *Microporous Mater.* **7**, 151 (1996).
35. Kunkeler, P. J., Moeskops, D., and van Bekkum, H., *Microporous Mater.* **11**, 313 (1997).